Single-Channel Kinetics, Inactivation, and Spatial Distribution of Inositol Trisphosphate (IP_3) Receptors in *Xenopus* Oocyte Nucleus

Don-On Daniel Mak and J. Kevin Foskett

From the Department of Physiology, University of Pennsylvania, Philadelphia, Pennsylvania 19104-6100

ABSTRACT Single-channel properties of the *Xenopus* inositol trisphosphate receptor (IP_3R) ion channel were examined by patch clamp electrophysiology of the outer nuclear membrane of isolated oocyte nuclei. With 140 mM K^+ as the charge carrier (cytoplasmic $[IP_3] = 10$ μM, free $[Ca^{2+}] = 200$ nM), the IP_3R exhibited four and possibly five conductance states. The conductance of the most-frequently observed state M was 113 pS around 0 mV and ~300 pS at 60 mV. The channel was frequently observed with high open probability (mean $P_o = 0.4$ at 20 mV). Dwell time distribution analysis revealed at least two kinetic states of M with time constants $\tau < 5$ ms and ~20 ms; and at least three closed states with τ ~1 ms, ~10 ms, and >1 s. Higher cytoplasmic potential increased the relative frequency and τ of the longest closed state. A novel "flicker" kinetic mode was observed, in which the channel alternated rapidly between two new conductance states: F_1 and F_2. The relative occupation probability of the flicker states exhibited voltage dependence described by a Boltzmann distribution corresponding to 1.33 electron charges moving across the entire electric field during F_1 to F_2 transitions. Channel run-down or inactivation ($\tau \sim 30$ s) was consistently observed in the continuous presence of IP_3 and the absence of change in $[Ca^{2+}]$. Some (~10%) channel disappearances could be reversed by an increase in voltage before irreversible inactivation. A model for voltage-dependent channel gating is proposed in which one mechanism controls channel opening in both the normal and flicker modes, whereas a separate independent mechanism generates flicker activity and voltage-reversible inactivation. Mapping of functional channels indicates that the IP_3R tends to aggregate into microscopic (<1 μm) as well as macroscopic (~10 μm) clusters. Ca^{2+}-independent inactivation of IP_3R and channel clustering may contribute to complex $[Ca^{2+}]$ signals in cells.

KEY WORDS: Ca^{2+} signaling • inositol phosphates • calcium release channel • patch clamp • signal transduction

INTRODUCTION

In many cell types, binding of ligands to plasma membrane receptors activates the hydrolysis of phosphatidylinositol 4,5-bisphosphate by membrane-bound phospholipase C, generating inositol 1,4,5-trisphosphate (IP_3).[1] IP_3 causes the release of Ca^{2+} from intracellular stores including the endoplasmic reticulum (ER) by binding to its receptors (IP_3R) (Taylor and Richardson, 1991; Berridge, 1993; Putney and Bird, 1993). Several types of IP_3R as products of different genes (Mignery et al., 1990; Yamamoto-Hino et al., 1994) with alternatively spliced isoforms (Mikoshiba, 1993; Taylor and Traynor, 1995) have been identified and sequenced. The IP_3Rs have ~2,700 amino acid residues in IP_3 binding, regulatory (modulatory) and transmembrane channel domains (Mignery and Südhof, 1990; Mikoshiba, 1993; Taylor and Traynor, 1995), and form tetramers (Mignery and Südhof, 1990). The putative transmembrane domains of the receptors have sequence homology with some of those in the ryanodine receptor (Taylor and Traynor, 1995), a muscle sarcoplasmic reticulum Ca^{2+} channel (Williams, 1992). Reconstitution of purified IP_3R demonstrated that the receptor itself is a Ca^{2+} channel (Supattapone et al., 1988).

Defining the details of the single-channel properties of the IP_3R has been hampered by its intracellular location. Single-channel studies have been accomplished by reconstituting the IP_3R channels (purified or in membrane vesicles) into planar lipid bilayers (Ehrlich and Watras, 1988; Bezprozvanny et al., 1991, 1994; Watras et al., 1991; Mayrleitner et al., 1991, 1995; Bezprozvanny and Ehrlich, 1993, 1994). However, because reconstitution protocols isolate the IP_3R from its native membrane environment and possibly disrupt normal protein–protein and protein–lipid interactions, channel properties and regulation of IP_3R observed in bilayers may not faithfully reflect the situation in situ. To circumvent these problems associated with recording currents through intracellular ion channels, we and others (Mak and Foskett, 1994; Stehno-Bittel et al., 1995) have applied the patch clamp technique to isolated cell nuclei. The rationale of this approach is the observed continuity of the ER with the outer membrane of the nuclear envelope (Dingwall and Laskey, 1992) and the

Address correspondence to Dr. Don-On Daniel Mak, Department of Physiology, University of Pennsylvania, Stellar-Chance Laboratories, Rm. 314, Philadelphia, PA 19104-6100. Fax: 215-573-8590; E-mail: dmak@mail.med.upenn.edu

[1] *Abbreviations used in this paper:* BAPTA, 1,2-bis(*O*-aminophenoxy)ethane-*N,N,N′,N′*-tetraacetic acid; BONS, basic oocyte nucleus solution; ER, endoplasmic reticulum; IP_3, inositol 1,4,5-trisphosphate; IP_3R, IP_3 receptor.

successful application of the patch clamp technique to the nuclear envelope despite the presence of nuclear pores (Mazzanti et al., 1990, 1991; Tabares et al., 1991; Bustamante, 1992, 1993, 1994; Matzke et al., 1992). Physiological, biochemical, and immunocytochemical studies have implicated the nuclear envelope as an IP_3-sensitive Ca^{2+} store in several cell types (Lin et al., 1994). Of particular relevance for the present study, the IP_3R has been localized to the nuclear envelope in *Xenopus laevis* oocytes (Parys et al., 1992, 1994; Kume et al., 1993; Callamaras and Parker, 1994). Patch clamp of the outer membrane of isolated *Xenopus* oocyte nuclei revealed IP_3-sensitive ion channel activities, providing the first demonstrations of the single-channel properties of IP_3R in its native membrane environment (Mak and Foskett, 1994; Stehno-Bittel et al., 1995).

In our initial study (Mak and Foskett, 1994), we demonstrated that one of the most frequently observed channels in outer nuclear membrane patches exposed to 10 μM IP_3 and 200 nM free Ca^{2+} in the pipette solution, was the IP_3R, as evidenced by its activation by IP_3 and inhibition by the competitive inhibitor heparin. This IP_3R was likely the type 1 isoform since this isoform has been localized to both the ER and nuclear envelope of *Xenopus* oocytes (Parys et al., 1992, 1994; Kume et al., 1993; Callamaras and Parker, 1994), and it is likely the only sub-type expressed by the oocyte (Kobrinsky et al., 1995). The *Xenopus* IP_3R was found to be weakly Ca^{2+}-selective, with ion permeabilities $P_{Ca}/P_K/P_{Cl}$ = 8:1:0.05. Multiple conductance states, current-voltage (*I-V*) relation in symmetric and asymmetric ionic conditions, some kinetic properties, and the inactivation or run-down in the continuous presence of IP_3 of the IP_3R channel were described. Some of these properties of the IP_3R in its native membrane environment were different from those described for rat cerebellar IP_3R reconstituted in lipid bilayers (Bezprozvanny et al., 1991; Watras et al., 1991; Bezprozvanny and Ehrlich, 1994, 1995). In this paper, we describe more detailed studies of the endogenous IP_3R in the *Xenopus* oocyte, characterizing for the first time the detailed kinetic properties of the channel and its inactivation, and the distribution of functional IP_3R channels in the outer nuclear membrane.

MATERIALS AND METHODS

Isolation of Individual Oocyte Nuclei

Maintenance of *Xenopus laevis*, surgical extraction of ovaries and storage of the extracted ovaries were described previously (Mak and Foskett, 1994). Stage VI oocytes (Smith et al., 1991) were isolated from the ovary just before the experiments and opened mechanically. The translucent nucleus was gently separated from the cytoplasmic material in the bathing solution and transferred to a culture dish containing the same solution on the stage of a microscope for patch-clamp experiments.

Patch Clamping the Oocyte Nucleus

The isolated nucleus was gently immobilized as described previously (Mak and Foskett, 1994). A patch pipette (5–20 MΩ when filled with 140 mM KCl) was placed so that its tip came into contact with the outer membrane of the nucleus, as indicated by an increased (≈10%) pipette resistance. Gigaseals formed (>80% success rate) when gentle suction (5–20 mmHg) was applied to the pipette. To estimate the duration of channel activity, current recording was started as soon as the seal resistance exceeded 200 MΩ (3–10 s after the pipette tip contacted the nucleus), before it attained its final stable value. Due to inactivation or run-down of the IP_3R channels (Mak and Foskett, 1994 and this study), all experiments were done in the "on-nucleus" configuration without excision of the patched membrane. No difference was detected in the current-voltage relation of the channels observed before and after excision of the membrane patches (Mak and Foskett, 1994; Fig. 1). This indicated that the cation composition of the solution in the perinuclear space between the inner and outer nuclear membranes is similar to that of the bath solution in these experiments. Following standard conventions, the applied potential is the potential difference between the pipette electrode and the reference bath electrode. Accordingly, positive current flowed from pipette outward. All patch clamp experiments were performed at room temperature under symmetrical ionic conditions with the pipette solution containing 10 μM IP_3.

Data Acquisition and Analysis

Single-channel currents were amplified with an Axopatch-1D amplifier (Axon Instruments, Foster City, CA) with anti-aliasing filtering at 1 or 5 kHz, transferred to a Macintosh Centris 650 via an ITC-16 interface (Instrutech Corp., Great Neck, NY), digitized at 2 or 12.5 kHz, respectively, and written directly onto hard disk by Pulse+PulseFit software (HEKA elektronik, Lambrecht, Germany). Data were analyzed (with further digital filtering when necessary) and fitted with theoretical curves using MacTac 2.0 (Skalar Inst., Seattle, WA), pCLAMP 6.0.2 (Axon Instruments), and Igor Pro 3 (WaveMetrics, Lake Oswego, OR).

Materials and Solutions

IP_3 and BAPTA (1,2-bis(*O*-aminophenoxy)ethane-*N,N,N′,N′*-tetraacetic acid) were from Molecular Probes (Eugene, OR); ATP (magnesium salt), EGTA, and inorganic salts were from Sigma Chem. Co. (St. Louis, MO). The standard solution contained 140 mM KCl, 10 mM HEPES, 3 mM $MgCl_2$, 1 mM MgATP, 1 mM BAPTA, 0.543 mM $CaCl_2$ at pH 6.95 with calculated free [Ca^{2+}] of 200 nM, and was used in all experiments unless specified otherwise. Free [Ca^{2+}] in various solutions was calculated using Maxchelator software (C. Patton, Stanford University, CA). K^+ was used as charge carrier since Ca^{2+} at high concentrations may inhibit IP_3R activity (Bezprozvanny et al., 1991). The basic oocyte nucleus solution (BONS) used previously (Mak and Foskett, 1994) had the same ionic composition but contained no MgATP.

RESULTS

Channel Identity

In symmetric standard solution, channels with multiple conductance states were observed in the oocyte outer nuclear membrane. The channel current-applied voltage (I-V) relation of the most-frequently observed conductance state M ("main") of the channel is nonlinear with rectification at high applied potentials (Fig. 1).

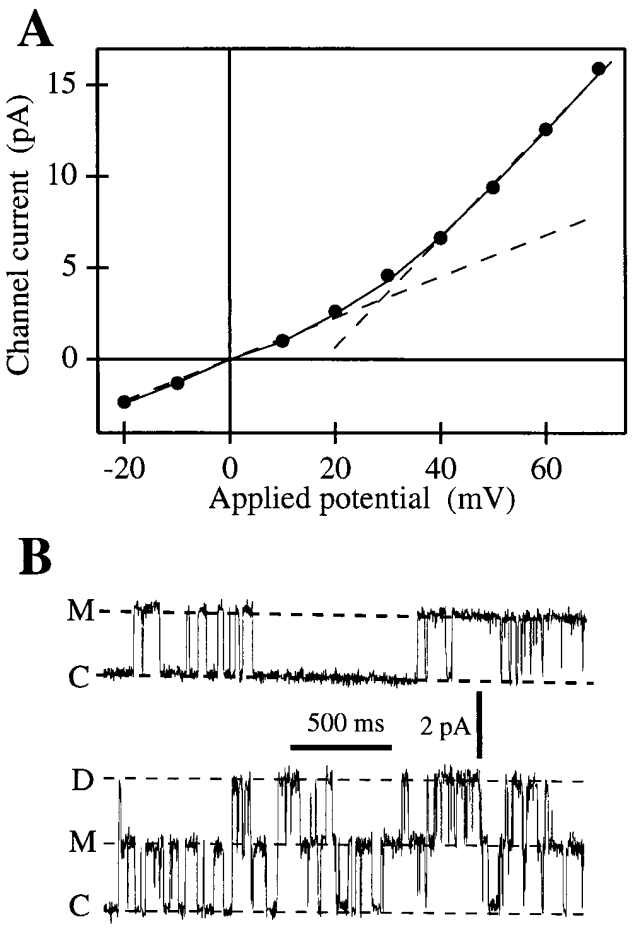

FIGURE 1. (*A*) I-V curve of the main state M of the IP_3R in the oocyte outer nuclear membrane. Channel current amplitudes in symmetric standard solution (*filled circles*) were evaluated as the difference between Gaussian peaks fitted to current amplitude histograms of current records containing the closed and main states (n = 12; filtered at 1 or 5 kHz). Current amplitude in an excised patch in symmetric basic oocyte nucleus solution obtained previously (Mak and Foskett, 1994) is also plotted (*solid line*). The dashed lines represent differential conductances of 113 pS at 0 mV and 300 pS at 60 mV, respectively. (*B*) Typical current traces of the IP_3R channel at 20 mV, showing closed (*C*), main (*M*), and double (*D*) states. Data was digitized at 2 kHz and filtered at 1 kHz.

The slope conductance of the channel around 0 mV was 113 pS, and gradually increased to ~300 pS around +60 mV. This I-V relation is practically identical to that of state M of IP_3R observed previously in symmetric BONS (Mak and Foskett, 1994). To confirm the identity of these channels as IP_3R, statistical means were used to determine the responses to IP_3. Multiple patches were obtained from nuclei (4–10 patches from each nucleus) in which the probability (P_d) of detecting the described channels in the presence of IP_3 was high (>0.5), with the pipette solution alternately containing either no IP_3 or 10 μM IP_3. Channels as described were observed in 20 of 26 patches with IP_3 from 6 different nuclei, but not observed in any of 14 patches with no IP_3. In a similar series of experiments with the pipette solutions containing either IP_3 or IP_3 together with 100 μg/ml heparin (a competitive inhibitor of IP_3R), channels as described were observed in 9 of 18 patches with IP_3 from 2 nuclei, but not in any of the 10 patches with IP_3 and heparin (Mak and Foskett, 1994).

Other channel activities were observed independent of the presence of IP_3 in the pipette solution. They were easily distinguished from IP_3R channels by their conductances (either >400 pS or ~20 pS), their linear I-V relation, and their gating kinetics.

IP_3R Localization in Clusters

A significant proportion (59/102) of the active patches (102 active/740 patches) in the standard solution in which IP_3R activities were detected contained multiple IP_3R channels, as identified by current records showing three or more equally spaced current levels, each corresponding to the conductance value of state M (Fig. 2). In contrast, only 19 patches exhibited just one open channel current level of state M. Two equally spaced current levels (M and D) were detected in 24 patches (Fig. 1 *B*). Whether such double-level records represent two channels or a substate of a single channel is discussed later. In either case, the high proportion of multiple-channel patches suggests that IP_3Rs are not distributed evenly over the surface of the outer nuclear membrane, but are localized in clusters (Fig. 3).

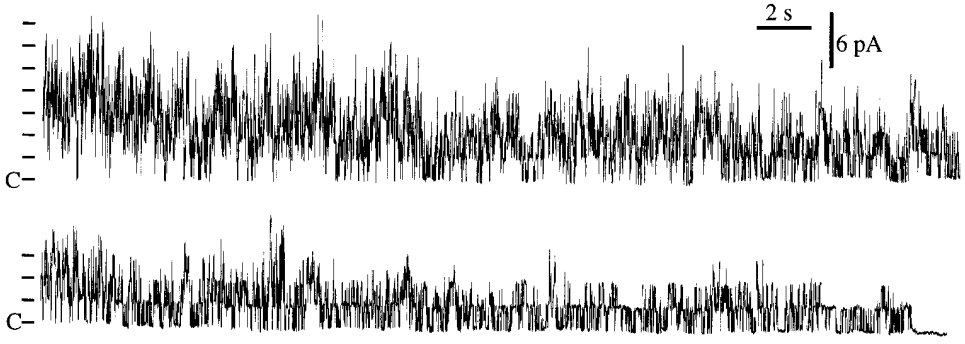

FIGURE 2. Typical multiple-channel current record showing seven equally-spaced current levels at the beginning of the recording. Channel activity duration for this record is 70.2 s (from the beginning of the record to the final closing event as the last observed channel inactivated). V_{app} was 20 mV. Data were digitized at 2 kHz and filtered digitally at 300 Hz.

In addition to the high frequency of observing patches with multiple channels, other data obtained also support the idea that the IP_3R exists in clusters. With the oocyte nucleus secured by a stabilizer (Mak and Foskett, 1994), video imaging enabled membrane patches to be repeatedly obtained from approximately the same area (± 2 μm). In 13 of 67 nuclei in which IP_3R activities were detected (137 nuclei examined), "macroscopic regions" on the membrane surface were defined in which P_d (0.74, n = 72) was significantly higher than the overall P_d (0.14, n = 740), or the P_d of other regions on the same nuclei (0.19, n = 52). Also, active patches obtained within such regions contained significantly ($P < 0.02$) more IP_3R channels (202 current levels in 53 patches) than all the other active patches (133 levels in 49 patches). In a 25 × 55 μm region, whose boundary was mapped by a large number of patches obtained, IP_3R activities were detected in all 7 patches obtained, with 6 patches showing more than one current level, whereas no IP_3R activity was detected in all 4 patches obtained outside the region. In another such region of similar size of another nucleus, multilevel IP_3R activities were detected in all 6 patches obtained, and IP_3R activity with only one current level was detected in 1 of 8 patches obtained outside the region. While the exact size and shape of such active regions could not be determined because each recording examined only a small membrane area (~1 μm^2), these results strongly suggest that besides the "microscopic clustering" (<1 μm in diameter) of the IP_3R channels that give rise to a high frequency of obtaining membrane patches with multiple channels, IP_3Rs are also organized into "hot regions" that can extend over several to tens of micrometers.

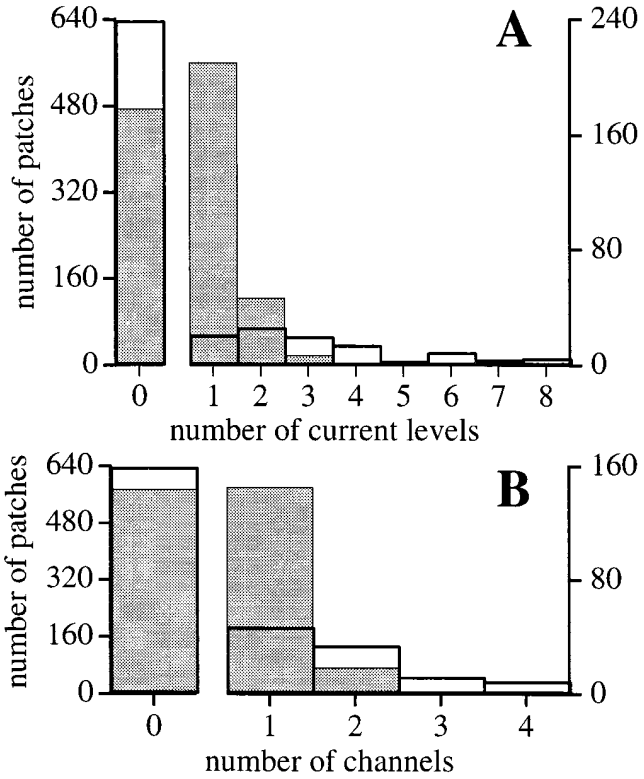

FIGURE 3. (*A*) Histogram analysis of current levels observed in 740 patches (*unshaded histogram with thick outline*). Also plotted (*shaded histogram with thin outline*) is the Poisson distribution with the same mean current level number per patch (0.44 current level/patch for 740 patches), calculated by assuming that each current level represents an individual IP_3R that exhibited only the M state and that the channels were evenly distributed on the outer nuclear membrane. (*B*) Histogram analysis of number of channels in the 740 patches (*unshaded histogram with thick outline*) assuming that all IP_3R channels observed exhibited the D state, such that every two current levels detected represents one channel. The theoretical Poisson distribution with the same mean channel number per patch (0.25 channel/patch for 740 patches) is also plotted (*shaded histogram with thin outline*). In both cases, the large number of observed multiple-channel patches compared with the number of observed single-channel patches suggests that the IP_3R channels are not evenly distributed in the outer nuclear membrane of oocytes.

Normal Kinetics of the IP_3R

The kinetics of the IP_3R observed in the standard solution in the present study (Figs. 1 *B* and 4) were charac-

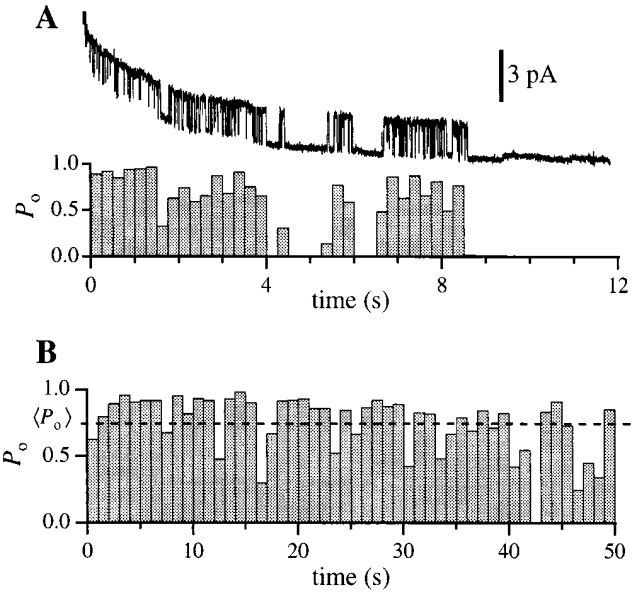

FIGURE 4. (*A*) Current trace and open probability histogram of a typical current record with the IP_3R channel in the main and closed states. Base-line current level fluctuated in the record because current recording was started before the gigaseal completely stabilized. The channel in the current record inactivated permanently by 9 s after seal formation. Bin width for the histograms is 0.25 s. (*B*) Open probability histogram for a single IP_3R with longer duration of channel activity. Bin width is 1 s. For both records V_{app} was 20 mV, data were digitized at 2 kHz and filtered at 300 Hz digitally.

terized by a relatively high open probability (P_o) (mean P_o = 0.4 at 20 mV for 15 experiments lasting a total of 582 s) and average open duration for state M of between 9 and 22 ms (n = 5; filtered at 1 kHz). Intrinsic inactivation or run-down of the IP_3R after exposure to IP_3 (data presented below) limited the number of long experiments available for detailed kinetic study. In those experiments with sufficient opening and closing events for kinetic analyses (n = 7), dwell time distribution histograms of the closed C and open M states typically had to be fitted with at least 2 exponential components each (Fig. 5). Since the dwell time distributions obviously extend beyond the resolution of our experiments, both states C and M might have exponential components with time constants shorter than 1 ms. Assuming that the channel kinetics are Markovian and steady throughout the duration of channel activity, the dwell time histograms indicated that there are at least two kinetically distinguishable main states with time constants $\tau < 5$ ms and ~20 ms. The channel also has at least two closed states with time constants τ ~1 and ~10 ms. Furthermore, in many experiments (>40%), periods of high channel activity were separated by quiescent (P_o = 0) periods that could last from several seconds to >10 s (Fig. 6 *A*). This indicated that the channel must also have at least one long closed kinetic state C_{long} with time constant >1 s.

In patches (n = 5) in which the IP_3R remained active long enough for kinetics to be observed at various applied potentials V_{app} (>15 s at each V_{app}), there was no consistent correlation between the dwell time distributions for the main and closed channel states and V_{app} (Fig. 5). In those patches (2/5) that showed current level D, the probability of observing the channel current in level D (P_D) also did not show noticeable correlation with V_{app} (Fig. 6 *B*). The only consistent effect of voltage on channel kinetics was an increase in the number and duration of long quiescent periods observed under higher V_{app} (Figs. 5 and 6 *A*), which tended to decrease the P_o averaged over the whole duration of channel activity at constant applied potential (Fig. 6). However, as shown in Fig. 6 *A*, long quiescent periods were often observed at low V_{app} as well. Detailed investigation of the voltage dependence of C_{long} kinetic state

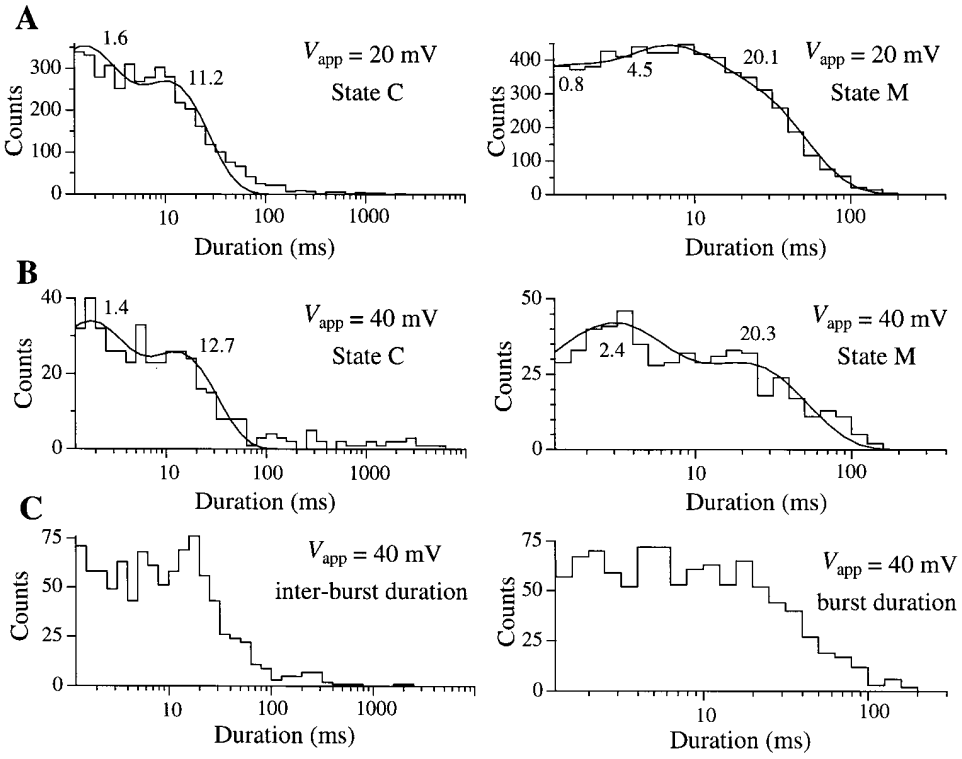

FIGURE 5. Dwell time histograms for the closed state C and open state M of the IP_3R at V_{app} = (*A*) 20 and (*B*) 40 mV, respectively. Only states C and M were observed in the single-channel current records used for this analysis. 6 records with total duration of 139.1 s were used for *A*, and 1 record with duration of 42.8 s was used for *B*. The smooth curves are theoretical probability density functions consisting of two exponentials fitted to the histograms by the maximum likelihood method (Sigworth and Sine, 1987). The time constants for the exponentials fitted are labeled in ms beside the corresponding peaks in the curves. (*C*) Duration histograms of inter-burst closed state and the activity bursts of an IP_3R channel in the flicker mode at V_{app} = 40 mV. The activity burst duration was defined as the interval between the departure of the channel from the closed state into either one of the flicker states (F_1 or F_2) and its subsequent return to the closed state for a period longer than 1 ms. Data were digitized at 2 kHz, filtered at 800 Hz and analyzed using MacTac software with channel dwell time corrected for the filtering (Colquhoun and Sigworth, 1995).

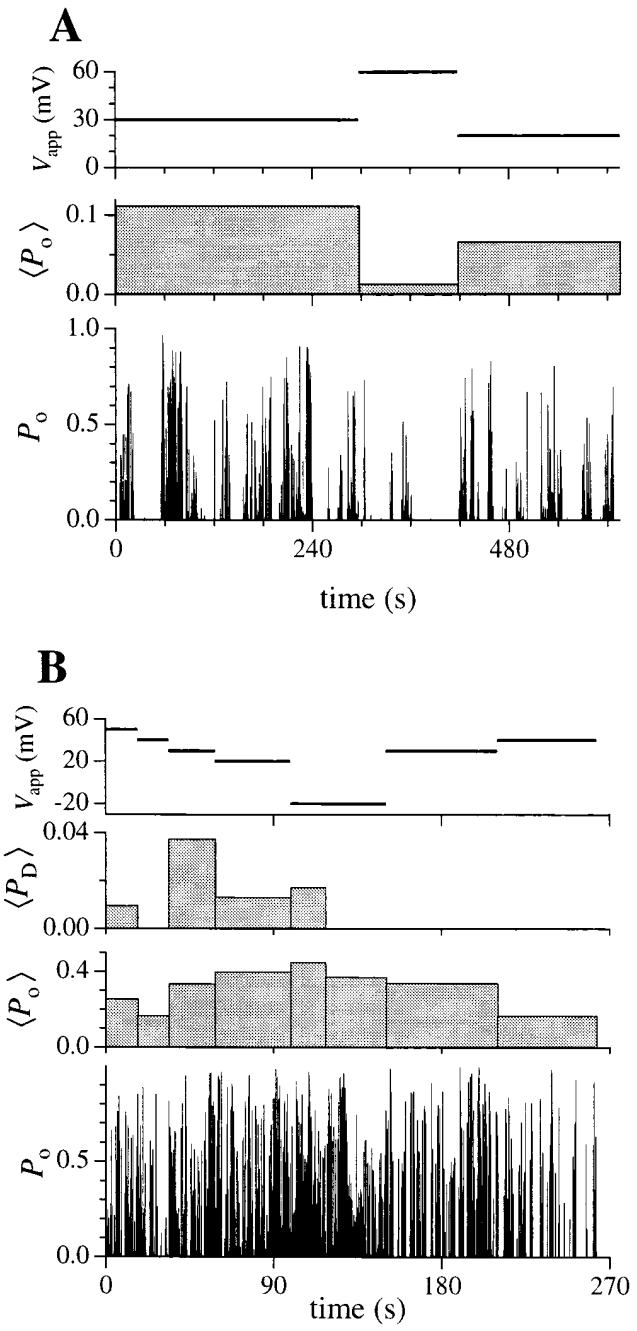

FIGURE 6. The effect of applied potential on IP_3R channel open probability. $\langle P_o \rangle$ is the overall open probability of the channel averaged over the interval during which the applied potential V_{app} was constant. Bin width of the P_o histogram is 0.25 s. The intervals (2–6 s) during which the applied potential was changed in the experiment were omitted in the graphs to avoid confusion. (*A*) A single-channel patch in which only states C and M were observed in the entire current record up to the failure of the gigaseal at $t = 615$ s. (*B*) A patch showing two equally-spaced channel current levels. The channel(s) observed inactivated at $t = 262$ s. $\langle P_D \rangle$ is the probability of observing the channel current in the higher level D, averaged over the interval indicated by the width of the bin. Channel current level D was not observed after $t = 117.5$ s. P_o is the probability of the channel being open, i.e., $P_o = P_D + P_M$, where P_M is the probability of observing the channel current in the main state level.

was hindered by the inactivation of the channel. As V_{app} increased, the quiescent periods increased and only a few periods of activity could be observed before the channel inactivated.

Conductance States of IP_3R

As in BONS (Mak and Foskett, 1994), in addition to state M, a rare state H ("half") with conductance half that of the main state M in the standard solution was observed briefly (duration <0.1 s) in 6 of 102 active patches. A current level corresponding to the state D ("double") described in Mak and Foskett (1994) with conductance twice that of state M was observed in 24 of 102 active membrane patches (Fig. 1 *B*). Two additional states with different conductances were observed in our present study, but only very rarely (<0.1% of total channel open time). These included a large state L (in 9 patches, Fig. 7 *A*) with conductance value ~1.3 times that of state M, and a small state S with conductance value ~0.7 times that of state M (in 5 patches, Fig. 7 *B*). The relation of state S to the IP_3R was established by observations of transitions between IP_3R state M and state S without channel closing (Fig. 7 *B*). Furthermore, both states L and S were only observed in patches in which the main IP_3R state M was also observed.

The issue of whether current level D is a true substate of a single channel or reflects the activity of two channels is complicated by the fact that its conductance is exactly twice that of the predominant state M. The large number of patches with two equally spaced current levels relative to that of single current-level patches (Fig. 3) suggests that current levels D and M are physically associated and that level D is likely not generated by the random inclusion of two channels in the patches. Several observations further suggest that the gating kinetics of IP_3R to levels M and D are highly correlated. Theoretically, two identical, independent active chan-

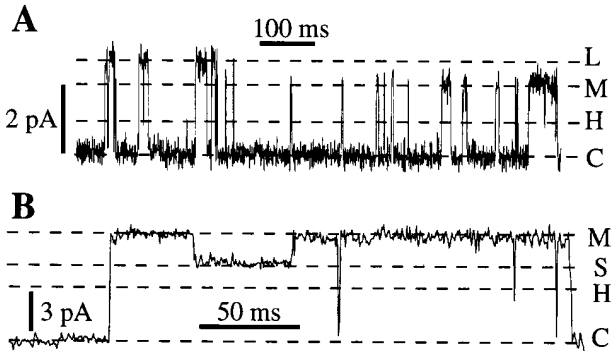

FIGURE 7. Current traces showing rarely observed conductance states L (*A*) and S (*B*) for channels in normal kinetic mode from 2 separate experiments. Data were digitized at 2 kHz and filtered at 1 kHz. $V_{app} = 20$ mV for (*A*) and 50 mV for (*B*).

nels should generate currents with open probabilities P_1 and P_2 (probabilities that one or both channels were open, respectively) described by the binomial probability distribution:

$$P_1 = 2\sqrt{P_2}\,(1 - \sqrt{P_2}).$$

However, of the 24 patches showing only current levels M and D, only one demonstrated an experimental probability of the channel current being at level M (P_M) that agreed with the theoretical probability P_1, calculated using the experimental probability that the channel current was at level D (P_D) as P_2 in the equation (Fig. 8 *A*). The other patches had P_M significantly different from the theoretical P_1 (Fig. 8 *B*). This suggests that most of the channel records showing current level D were not caused by two identical, independent channels located in the same membrane patch. In most patches with current level D, there were long periods (over several seconds) during which only current level M was observed (*t* after 117.5 s in Fig. 6 *B*, and between 110 and 160 s in Fig. 8 *B*). The P_o ($P_M + P_D$) during these periods was not noticeably different from that during those periods in which level D was observed (Figs. 6 *B* and 8, *A* and *B*). Also, the dwell time distributions for the closed state C in the presence and absence of current level D were practically indistinguishable (data not shown). Furthermore, two patches showing current levels M and D exhibited long quiescent periods, with levels D and M both occurring within the relatively short periods of channel activities (Fig. 8 *C*). These observations were unlikely to be caused by two independent channels in the patched membrane even if the channels had erratic open probabilities with long quiescent periods. They probably reflect the presence of either two interdependent cooperative channels each exhibiting state M only, or a single channel with true states M and D.

Inactivation of the IP_3R

A prominent feature of the IP_3R channel activities observed in our experiments was inactivation or run-down of the channels in the continuous presence of IP_3 in the pipette, in standard solution (Fig. 4 *A*) as well as BONS (Mak and Foskett, 1994). Channels could be activated upon gigaseal formation for >2 h after the nucleus was isolated, indicating that inactivation required activation by IP_3. Inactivation was generally abrupt, with no significant difference between P_o of a channel just before inactivation and just after it had been activated (Figs. 4 and 6 *B*). However, the rapidity of the onset of inactivation (usually <2 min) prevented the detailed analysis necessary to determine if the channel kinetics (dwell time distributions of states C and M) varied significantly during the course of inactivation.

In ~10% of patches (9/102) with IP_3R channel activities, the channels could be reactivated after inactivation, by an increase in V_{app} of 20–40 mV (Fig. 9). In two of these patches, channel inactivation was reversed twice by repeated jumps in V_{app}, using a voltage proto-

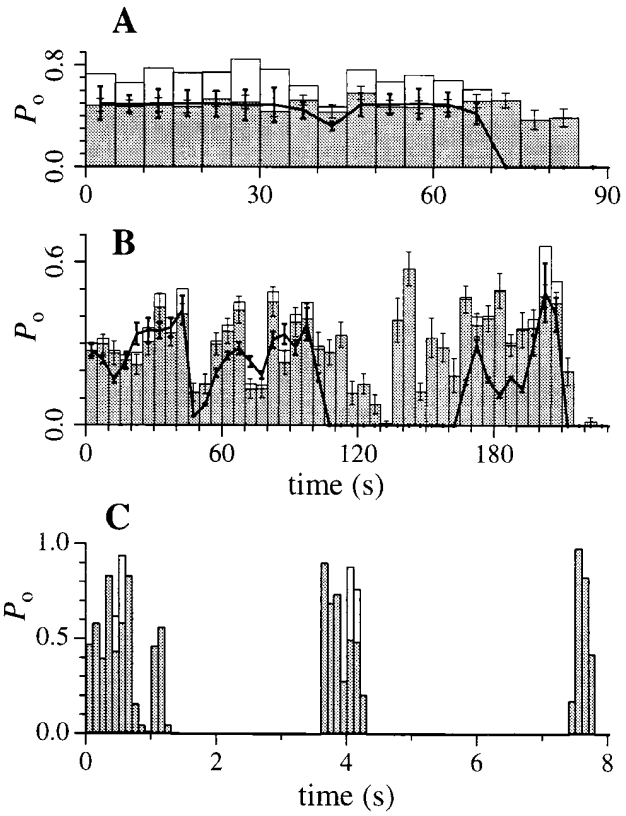

FIGURE 8. Open probability histograms for experiments in which two evenly spaced current levels (*M* and *D*) were detected. (*A* and *B*) Histogram bin width is 5 s. Unshaded histogram bars are the measured probability of the channel current in level D (P_D); shaded bars with thin error bars are the measured probability (± SEM) of the channel in state M (P_M). Assuming that current level D is caused by two independent and equivalent channels contained in the same membrane patch opening to state M simultaneously, the theoretical probability P_1 of the channel current being at the level corresponding to a single channel in state M is given by the binomial distribution,

$$P_1 = 2\sqrt{P_2}\,(1 - \sqrt{P_2}).$$

The solid lines represent the theoretical probability P_1 evaluated using the measured probability P_D as P_2. The thick error bars represent the errors in P_1 evaluated from the SEM of P_D. In *A*, the measured P_M agreed well with the theoretical P_1 calculated from P_D, indicating that the patch probably contained two independent and equivalent channels until one channel inactivated after $t = 70$ s. In *B*, which is typical of the majority of channel current records showing two evenly spaced current levels, P_M and P_D measured did not obey the binomial distribution expected for two independent and equivalent channels. (*C*) Open probability histogram of an experiment with current level D that exhibited long quiescent periods. Histogram bin width is 0.1 s. Unshaded histogram bars represent P_D; shaded bars represent P_M.

col similar to that shown in Fig. 9. Thus, an active IP_3R can enter at least two distinguishable inactivated states: one (I_{Vdep}) from which it can be reactivated by a jump in V_{app} (first inactivation in Fig. 9), and an irreversible one (I_{irr}) from which it cannot exit in the continuous presence of IP_3 under our experimental conditions (second inactivation in Fig. 9). In all our experiments, V_{app} was pulsed several times after channel inactivation, as in Fig. 9, to ensure that the observed channels had entered the irreversible inactivated state I_{irr} before the experiments were terminated.

The histogram of the duration of channel activity in patches with only one open channel current level M (Fig. 10 *A*) could be fitted by one exponential function with a time constant of 21.1 ± 0.6 s (n = 24, including six experiments that had previously been reactivated by a jump in V_{app}). This indicates that channel inactivation is probably a Markovian process with a time-independent probability for an active channel to become inactivated under constant experimental conditions. As IP_3R activation by exposure to IP_3 probably occurred some time before the seal resistance became high enough for the channel current to be monitored, it was impossible to determine the time of channel activation with accuracy greater than ±5 s, the average time that elapsed from the positioning of the micropipette containing IP_3 onto the nuclear membrane to the formation of the gigaseal. Thus, exponential components of inactivation with time constants shorter than 10 s could not be observed properly in our experiments. Also, since each experiment surveyed at most a few active channels, inactivation components with low relative weights and/or long time constants could not be observed properly due to the small sample size.

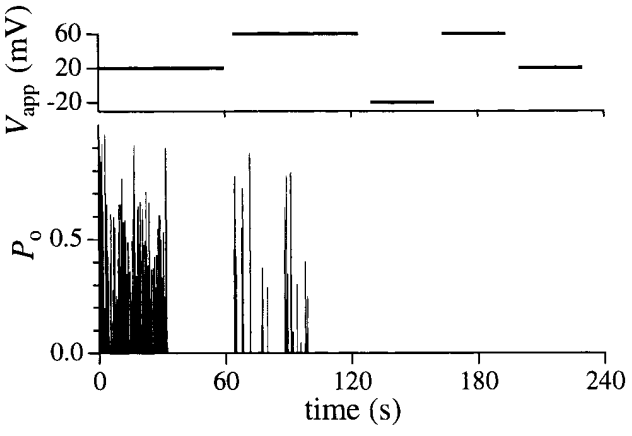

FIGURE 9. Open probability (P_o) and applied voltage (V_{app}) graphs of an experiment showing the two different types of channel inactivation: the voltage-reverted inactivation occurring at t = 32.25 s that was reversed by the increase of V_{app} from 20 to 60 mV at t = 60.0 s; and the irreversible inactivation occurring at t = 99.0 s. Bin width of the histogram is 0.25 s.

The duration of channel activity in patches with more than two equally-spaced channel current levels (from three to eight levels) was defined as the duration between the formation of the gigaseal (when seal resistance exceeded 200 MΩ) and the last observed channel closing event. Assuming that the channels in the same patch were identical and inactivation was Markovian with a single exponential component of time constant τ, the probability that an active channel observed at the time of seal formation (t = 0) becomes inactivated by time t is $\propto 1 - e^{-(t/\tau)}$. The probability that all of the k channels in a multi-channel patch are inactivated by time t is $\propto [1 - e^{-(t/\tau)}]^k$. Thus the probability that any channel in the k-channel patch remains active by time $t \propto \{1 - [1 - e^{-(t/\tau)}]^k\}$. In 41 experiments showing three or more open channel current levels (no reactivated experiments), the average number of current levels ob-

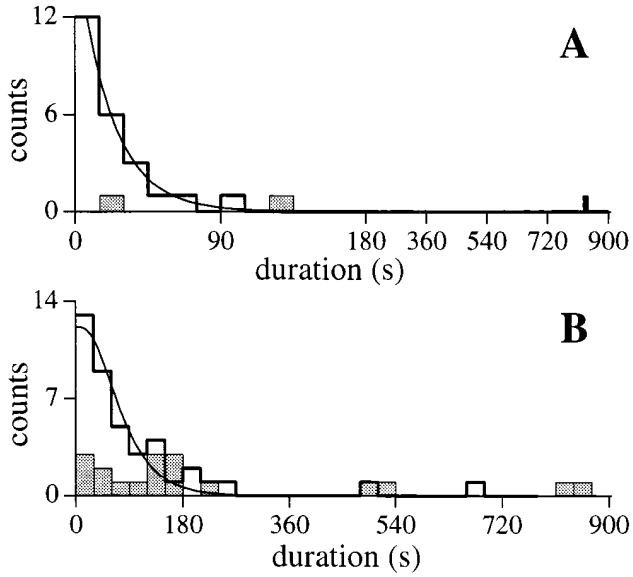

FIGURE 10. Channel activity-duration histograms of the IP_3R for (*A*) single-channel experiments in which only one channel current level (state M) was observed (n = 24, including six inactivations after reactivation by a voltage jump); (*B*) multiple-channel experiments in which three or more channel current levels were observed (n = 41, including six inactivations after reactivation by a voltage jump). Note the compressed time scale of (*A*) after t = 180 s. The measured duration of channel activity was the duration between the formation of the gigaseal (when seal resistance exceeded 200 MΩ) and the last observed channel closing event. The smooth curve in *A* is a single exponential functions fitted to the activity duration histogram with time constant of 21.1 ± 0.6 s. The smooth curve in *B* represents the theoretical functions fitted to the activity duration histogram for k = 4 with time constant of 41 ± 3 s. The theoretical fits for k = 3, 5, and 6 are very similar in shape, with different values for the time constant. Experiments in which the gigaseal broke before the channel(s) inactivated (n = 3 and 18 for *A* and *B*, respectively) were excluded from the activity duration histograms. Their duration distributions (*shaded histograms*) showed that failure of the gigaseal probably does not cause any significant systematic bias in the activity-duration histograms.

served was 4.63. The values of τ derived from the best fit of the theoretical equation to the duration histogram (Fig. 10 *B*) were 47, 41, 38, and 35 s (± 3 s) for k = 3, 4, 5 and 6, respectively. The statistically significant difference between the time constants for channel inactivation in single and multiple-channel patches ($P <$ 0.001 even assuming k = 6) suggested that IP_3R channels in multiple-channel patches do not inactivate independently, since they persist longer after IP_3 activation than those in single-channel patches.

Flicker Kinetics of the IP_3R

In ~25% of active patches (26/102), the channels also exhibited a radically different kinetic mode. In this "flicker" mode, a channel demonstrated bursts of activity during which it alternated rapidly between two new conductance states: F_1 and F_2 (Fig. 11 *B*). Between the bursts of activity, the channel exhibited a relatively long closed state. Direct transitions between either of the flicker states (F_1 and F_2) and the closed state (C) were observed (Fig. 11 *C*). Channels were observed to convert spontaneously between flicker and normal modes, often several times in the same experiment. The channels some times changed directly between the flicker states (F_1 and F_2) and state M in the normal mode without closing (Fig. 11 *C*). Channels were found in the flicker mode at the formation of the gigaseal (3/26) or they entered the flicker mode from the normal mode spontaneously (10/26); in half of the experiments with channels in the flicker mode, the flicker activity appeared after the channels were activated by a jump in V_{app} (n = 13, including two patches in which the channel was already in flicker mode before undergoing voltage-reversible inactivation and six patches with no recorded channel activity before the jump in V_{app}). Channels in the flicker mode irreversibly inactivated directly (n = 8), or subsequent to conversion to the normal mode (n = 13). (The gigaseal broke before channel inactivation in the remainder of the experiments that exhibited the flicker channel activity.)

In two experiments in which the channel remained in the flicker mode for an extended period (>200 s), a change of V_{app} from positive to negative (20 mV to −20 or −40 mV) caused the channel to close completely. Channel activity only resumed (in the flicker mode) when V_{app} was returned to positive. Channels were never observed in the flicker mode under negative V_{app}. This contrasts with the channels in the normal mode, which were active in both positive and negative V_{app}.

The duration distribution of the inter-burst closed state in the flicker mode (Fig. 5 *C*) was comparable to that of the closed state in the normal kinetic mode under the same V_{app} (Fig. 5 *B*). This suggests that the closed states in the flicker and normal modes are kinetically indistinguishable. The increases in number and duration of long quiescent periods under higher V_{app} were also observed for channels in the flicker mode, as for those in the normal mode. The duration of the bursts of activity of an IP_3R channel in the flicker mode (Fig. 5 *C*) had a distribution which was comparable to that of state M in the normal kinetic mode under the same V_{app} (Fig. 5 *B*).

The current levels for the states C, F_1, and F_2 and their occupation probability distributions were determined from the current amplitude histogram (Fig. 12 *A*). The count of current data points was fitted by the sum of three Gaussian functions:

$$\sum_s W_s \exp\{-[(i - i_s)/\sigma_s]^2\}$$

where s represents the states C, F_1, and F_2 (Root and MacKinnon, 1994), and W_s are the relative weights of the Gaussian functions. The mean current level for state s was taken to be the peak current value i_s of the corresponding Gaussian function. The channel current amplitude I_{F1} for state F_1 is then ($i_{F1} - i_C$), and I_{F2} for state F_2 is ($i_{F2} - i_C$). The ratio of the areas under the F_1 and F_2 Gaussian curves: $(W_{F2}\,\sigma_{F2})/(W_{F1}\,\sigma_{F1})$ was used as the relative occupational probability P_{F2}/P_{F1} of the flickering states F_1 and F_2 during the bursts of channel

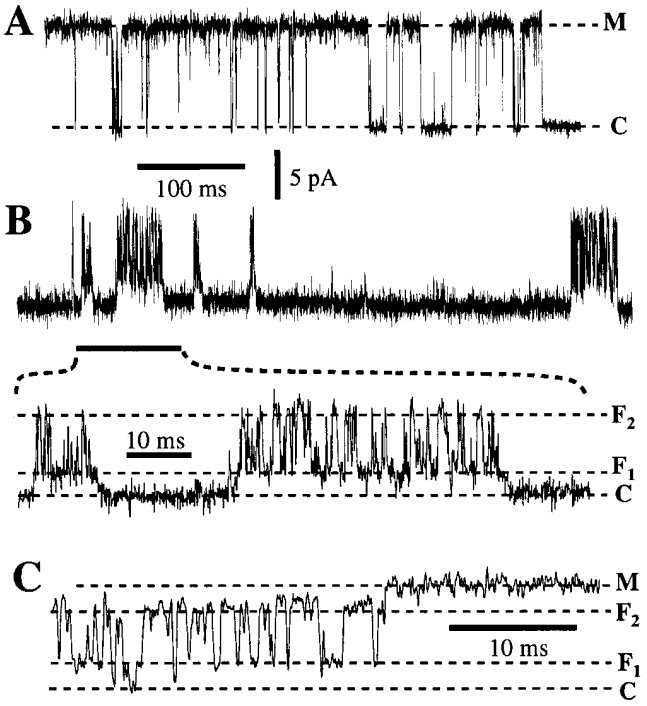

FIGURE 11. Typical current trace of an IP_3R channel (*A*) in the normal kinetic mode (*B*) in the flicker kinetic mode with bursts of activities and (*C*) in a transition from flicker mode to the normal mode without closing. The dashed lines indicate the current levels of the various conductance states. V_{app} was 50 mV. Data were digitized at 12.5 kHz and filtered at 5 kHz.

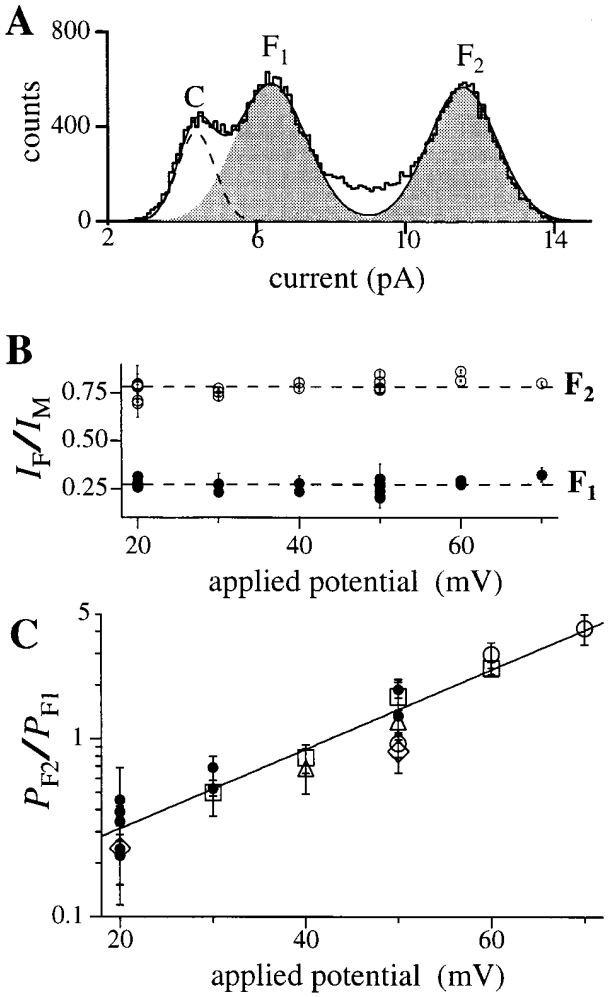

FIGURE 12. (*A*) Current amplitude histogram of a channel in the flicker kinetic mode. Segments of current traces during which the channel showed bursts of activities were selected to generate the histogram with bin width of 0.1 pA. V_{app} was 50 mV. Data were digitized at 12.5 kHz and filtered at 5 kHz. Theoretical fit to the histogram (*smooth curve*) is the sum of three Gaussian functions representing the closed state C (*dashed curve*), and the flicker states F_1 and F_2 (*shaded areas*). (*B*) Ratios of the channel current amplitude I_{F1}/I_M and I_{F2}/I_M under various applied potentials. The current amplitudes I_{F1}, I_{F2}, and I_M used for each data point were obtained in the same patch clamp experiment. Solid circles represent I_{F1}/I_M and open circles I_{F2}/I_M. Dashed lines indicate the mean ratios assuming no voltage dependence (0.27 for I_{F1}/I_M and 0.78 for I_{F2}/I_M). Most of the error in the ratios came from the fitting of the channel current amplitude histogram with the Gaussian functions. (*C*) Voltage dependence of the relative occupation probability of the flicker channel states P_{F2}/P_{F1}. Each type of open symbol (*squares*, *triangles*, *circles*, and *diamonds*) represents a series of data points obtained from the same single-channel patch. Filled circles are data points each from an individual patch at only one voltage. The straight line is the theoretical fit assuming that the occupation probability follows a Boltzmann distribution. The larger error in the data points for 20 mV is due to difficulty in fitting the Gaussian function to the scarce F_2 state.

activity. The deviation of the current amplitude histogram from the theoretical fit between i_{F1} and i_{F2} in Fig. 12 *A* was an artifact caused by filtering and was reduced by raising the filtering frequency. However, the relevant features of the theoretical fit, i.e., the ratio between the areas of the F_1 and F_2 Gaussian peaks (W_{F2} σ_{F2})/(W_{F1} σ_{F1}) and the location of the Gaussian peaks i_C, i_{F1}, and i_{F2} were not significantly affected by the filtering frequency (between 1 and 5 kHz).

The current amplitude ratios $I_{F1}/I_M = 0.27 \pm 0.01$ and $I_{F2}/I_M = 0.78 \pm 0.01$ (I_M was determined from current amplitude histograms of channels in the normal mode) showed no systematic voltage dependence (Fig. 12 *B*). Since state M of the channel in the normal kinetic mode had a nonlinear I-V relation (Fig. 1 *A*), the I-V relation for the flicker mode must also follow the same nonlinear relation over the observed voltage range. This result further confirms that the channel activity in the flicker mode was generated by the IP_3R.

The relative occupation probability of the flicker states P_{F2}/P_{F1} exhibited a voltage dependence (Fig. 12 *C*), which could be fitted theoretically by a Boltzmann distribution $P_{F2}/P_{F1} \propto \exp(z\, e\, V_{app}/kT)$ with $z = 1.33 \pm 0.05$ corresponding to an equivalent of 1.33 electron charges moving across the entire applied transmembrane electric field when the channel changes from the configuration of state F_1 to that of state F_2. An increase of 19.5 ± 0.7 mV in V_{app} will cause an *e*-fold increase in P_{F2}/P_{F1}. The voltage range of our analyzed data was restricted at high V_{app} by the occurrence of long interburst quiescent periods, which limited the amount of data that could be obtained, and at low V_{app} due to the difficulty of resolving the F_1 and C.

The applied potential affected the dwell time distributions of both flicker states. Increasing V_{app} shortened the mean dwell time of F_1 (Fig. 13 *A*) while lengthening that of F_2 (Fig. 13 *B*). Only one exponential component was resolved for each flicker state. Thus, in the simplest model, the channel has one kinetic state corresponding to F_1 and one corresponding to F_2. The channel passes through an activated state F* during the transition between F_1 and F_2. Since the $F_1 \leftrightarrow F_2$ transitions are the predominant transitions (>95%) involving the flicker states, by the Arrhenius theory, the time constant τ_{F1} of state $F_1 \propto \exp[(-z\, e\, d_1\, V_{app})/kT]$, where ($z\, e\, d_1\, V_{app}$) is the voltage-dependent part of the activation energy of the $F_1 \rightarrow F_2$ transition, and $d_1\, V_{app}$ is the fraction of the membrane potential that the charge $z\, e$ experiences when the channel configuration changes from F_1 to F*. Similarly, $\tau_{F2} \propto \exp[(z\, e\, d_2\, V_{app})/kT]$. Assuming that the value of 1.33 for z deduced from P_{F2}/P_{F1} is the same as the ones for $F_1 \rightarrow F^*$ and $F^* \rightarrow F_2$, the voltage dependence of the time constants of the flickering states (Fig. 13 *C*) gave $d_1 = 0.64 \pm 0.07$ and $d_2 = 0.38 \pm 0.07$.

DISCUSSION

The Conductance States of IP_3R

The *Xenopus* IP_3R ion channel is a multi-conductance cation channel in its native membrane environment, possessing at least four, and possibly five open-channel conductance states. A predominant state M was ~113 pS at low voltages (between ± 20 mV) in the presence of 140 mM K^+. The conductance of state M is twice that of a state H within experimental error (Mak and Foskett, 1994). Whether current level D actually represents a separate conductance state of the IP_3R cannot be determined conclusively at present. Our analysis indicates an apparent association or cooperativity between levels D and M, but these features may indicate either that D is a true sub-state or a reflection of interactions between two IP_3R, each with state M only. Such interactions between IP_3R channels may also exist in multichannel clusters. Conductance states L and S (~150 pS and 80 pS between ± 20 mV, respectively) were also detected in the current studies. A previous study using similar conditions (Stehno-Bittel et al., 1995) reported four states with conductances of 244 pS, 172 pS, 126 pS, and 90 pS, the 172 pS state being predominant. Assuming that this 172 pS state is the one we term M, the relative conductances of the other states compared to the predominant one are: 1.42, 0.73, and 0.52, respectively. These values agree reasonably well with the conductances of the states L, S, and H relative to state M in our studies, suggesting that the larger conductances reported by Stehno-Bittel et al. (1995) may be explained by their failure to observe and take into account the non-linear behavior of the I-V relation (Fig. 1). Four equally spaced conductance states of the mammalian type 1 receptor have been observed in reconstitution experiments (Watras et al., 1991). Considering the relative conductances of those states, it is possible that the first, second, and fourth level observed in the reconstitution experiments represent states H, M, and D in our experiments. However, reconstituted IP_3R occupied the first, second, and third conductance states with similar frequencies (29, 35, and 35%), whereas the fourth state was rarely observed (1%) (Watras et al., 1991). In its native membrane environment in our experiments, state H was rarely observed and no state corresponding to the third state was observed (Mak and Foskett, 1994 and present data).

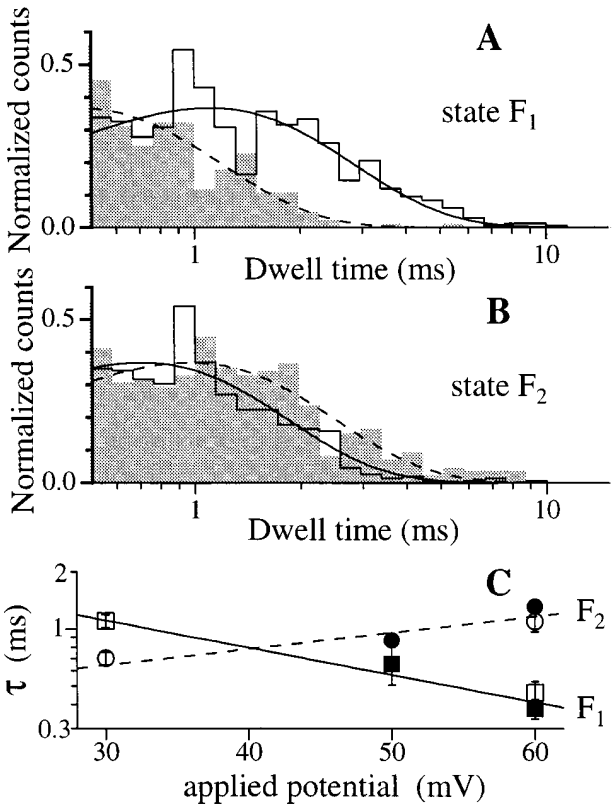

FIGURE 13. Effect of applied potential on the dwell time distributions of the flicker states F_1 and F_2. In *A* and *B*, V_{app} = 30 mV for the unfilled histograms, and the solid curves are the theoretical probability density functions each with one exponential component fitted using the maximum likelihood method (Sigworth and Sine, 1987). V_{app} = 60 mV for the shaded histograms and the dashed curves are their fitted single-exponential probability density functions. The transition counts were normalized so that the peaks of the fitted probability density functions have the same height. There are 784 and 209 transitions for 30 and 60 mV, respectively, in *A*; and 543 and 380 transitions for 30 and 60 mV, respectively, for *B*. Analysis was done on data digitized at 12.5 kHz and filtered at 2 kHz using pClamp 6.0.2. (*C*) is the graph of the time constants τ of the theoretical probability density functions fitted to the dwell time histograms of the flicker states under various applied potentials. Squares are time constants for F_1 and circles are for F_2. Open and filled symbols are from two different experiments. The lines are theoretical time constant values fitted according to the Arrhenius theory.

Kinetic Features of the IP_3R

Kinetic analysis of the open (M) and closed (C) states dwell-time distributions of IP_3R reveals at least two kinetic states for M with τ of <5 and ~20 ms, respectively; and at least three kinetic states for C with τ of ~1 and ~10 ms and >1 s, respectively. The long open kinetic state (τ ~20 ms) observed in the present study is longer and occurred more frequently than previously reported (Mak and Foskett, 1994). Its time constant is also considerably longer than that observed for the reconstituted IP_3R (Watras et al., 1991), although it is similar to that observed for the reconstituted ryanodine receptor (20 ms; Smith et al., 1986). This latter point suggests that it may not be possible to generalize (Bezprozvanny and Ehrlich, 1994) about the physiological importance of different kinetic behaviors of the two channels in cells which express both ryanodine receptors and IP_3R. The reasons for the marked kinetic dif-

ferences of the channel gating we previously observed compared with those reported here are unknown. ATP in mM concentrations affects the open probability of the reconstituted IP_3R (Bezprozvanny and Ehrlich, 1993; Missiaen et al., 1994). The experiments described in our previous report were performed in BONS in the absence of MgATP whereas most experiments in the present study were performed in the presence of 1 mM MgATP. Nevertheless, this variable is unlikely to account for the kinetic changes since similar channel kinetics, including high P_o and long open duration, were also observed when we removed MgATP from our solution (unpublished data). To identify any possible effect on channel kinetics of the BAPTA (Richardson and Taylor, 1993; Combettes et al., 1994) experiments were performed in symmetrical low BAPTA solution (0.1 mM BAPTA, $n > 20$) or EGTA-buffered solution (75 μM EGTA, $n = 8$) (data not shown). No substantial differences were observed in the I-V relation, P_o distribution, open and closed state kinetics, or inactivation of the channel. The IP_3R channel kinetics may depend on factors, such as redox (Kaplin et al., 1994) or phosphorylation (Taylor and Richardson, 1991; Joseph, 1995) states of the receptor, not adequately controlled between our previous and current experiments.

A high potential on the cytoplasmic side of the channel increased both the relative frequency of occurrence of the long closed kinetic state and its mean dwell time. Both voltage effects decrease the mean P_o of the channel at high cytoplasmic potentials. This voltage dependence is consistent with that exhibited by reconstituted cerebellar IP_3R in bilayers (Watras et al., 1991), IP_3-sensitive channels in beet vacuole (Alexandre et al., 1990), and the ryanodine receptor (Percival et al., 1994). In contrast, Stehno-Bittel et al. (1995) reported that the *Xenopus* IP_3R exhibited a higher P_o under more positive cytoplasmic potentials. We have no explanation for this discrepancy. With K^+, Na^+, and Cl^- ions distributed evenly on either side, as determined by electron probe x-ray study, there is probably little potential difference across the sarcoplasmic reticulum membrane (Somlyo et al., 1977). If the ionic distribution and transmembrane potential of the ER are similar, the voltage dependence of the IP_3R detected here may not have physiological significance. However, without independent measurements of the ER membrane potential, it remains possible that steady-state transmembrane voltages or transient shifts of membrane potential due to gating of ER membrane ion conductances, for example during activation of the IP_3R, do exist and influence IP_3R kinetic properties and P_o. In any case, the voltage sensitivities may provide insights into the gating mechanisms observed under low-voltage conditions.

The P_o of IP_3R measured in our experiments is significantly higher than the maximum values previously reported for single-channel measurement of IP_3R either in the nuclear membrane of oocytes (Mak and Foskett, 1994, $P_o \sim 0.1$; Stehno-Bittel et al., 1995, $P_o < 0.3$) or reconstituted in lipid bilayers from isolated vesicles (Bezprozvanny et al., 1991; Watras et al., 1991; Bezprozvanny and Ehrlich, 1993, 1994; $P_o \sim 0.1$) or purified protein (Mayrleitner et al., 1995; $P_o < 0.3$). In some current records in the present study, P_o remained close to 1.0 for seconds or even tens of seconds (Fig. 3). This observation demonstrates that the P_o of the IP_3R can switch from 0 in the absence of agonist to nearly unity when IP_3 binds, under suitable conditions. This all-or-none behavior would enable the IP_3R to mediate a rapid flux of Ca^{2+} out of intracellular Ca^{2+} stores, and thus it may contribute to the sharp rapid rise in cytoplasmic Ca^{2+} concentration observed in cells in response to IP_3-generating stimuli (Miyazaki, 1988; Meyer et al., 1990; Finch et al., 1991; Parker et al., 1996). The combined influences of the IP_3R channels' high conductance and P_o may be expected to result in high concentrations of Ca^{2+} in the immediate vicinity of the cytoplasmic face of even a single channel. Elevated levels of cytoplasmic Ca^{2+} concentration may inhibit Ca^{2+} flux through the IP_3R (Bezprozvanny et al., 1991; Marshall and Taylor, 1993; our unpublished observations). However, it is very unlikely that the long quiescent intervals corresponding to C_{long} reflect negative Ca^{2+} feedback on the channel. Since $[Ca^{2+}]$ was buffered at 200 nM in the pipette and bathing solutions, the amount of Ca^{2+} flux through the channel in the present experiments was small, particularly with positive potentials on the cytoplasmic side. It is unlikely therefore that any significant elevations in $[Ca^{2+}]$ occurred adjacent to the cytoplasmic side of the channel in our studies. Thus, the kinetic behavior of the IP_3R, at least in response to high IP_3 concentrations, is predicted to result in complex local cytoplasmic $[Ca^{2+}]$ signals by virtue of both feedback by $[Ca^{2+}]$ as well as intrinsic gating behavior of the channel.

Inactivation of IP_3R

An apparent inactivation of the IP_3R was consistently observed in our experiments. The channel activity disappeared with a time constant of ~30 s, in the continuous presence of IP_3 in the micropipette, and in the absence of local change in $[Ca^{2+}]$ (as discussed above). Some (10%) channel disappearances could be reversed by an increase in the applied potential. In those cases, the channels must have entered a true inactivated state (I_{Vdep}), remaining functionally intact inside the membrane patch. However, the majority of the channels, once inactivated, could not be reactivated during the course of the experiment. Since inactivation was not reported for IP_3R reconstituted in lipid bilayers (Ehrlich

and Watras, 1988; Bezprozvanny et al., 1991; Mayrleitner et al., 1991; Watras et al., 1991; Bezprozvanny and Ehrlich, 1994; Mayrleitner et al., 1995), it is possible that the irreversible disappearance of channel activity we observed is an artifact (run-down) caused by the isolation of IP_3R in the special environment of the patched membrane. However, neither non-IP_3R channels observed in our experiments (data not shown) nor the cystic fibrosis transmembrane conductance regulator $C1^-$ channel observed by similar patch clamping of isolated mammalian nuclei (Pasyk and Foskett, 1995) exhibited this behavior. Furthermore, recent patch-clamp measurements of purified IP_3R (Thrower et al., 1996) using the "tip-dip" technique (Coronado and La-torre, 1983) revealed no rapid disappearance of IP_3R activity in lipid bilayer patches isolated on micropipette tips (Thrower, E., and A.P. Dawson, personal communication). Thus, by itself, the membrane environment in a patch clamp experiment appears to be insufficient to cause the disappearance of IP_3R channel activity we observe. In permeabilized hepatocytes, inactivation of Mn^{2+} fluxes through the IP_3R in the ER in the continuous presence of IP_3 was observed (Hajnóczky and Thomas, 1994) which had a time constant comparable to that measured for the disappearance of IP_3R channel activity in our experiments. Therefore, it seems most likely that the irreversible disappearance of channel activity observed in our experiments is caused by the IP_3R channels entering a true inactivated state (I_{irr}) from which they cannot exit in the presence of a constant concentration of IP_3. This inactivated state I_{irr} may correspond to an inactive, high IP_3-affinity state (Piétri et al., 1990; Hilly et al., 1993; Watras et al., 1994) into which the IP_3R converts after prolonged exposure to IP_3R even in the presence of low $[Ca^{2+}]$ (Coquil et al., 1996). The reported time course for this conversion in isolated sheep cerebellar microsomes ($t_{1/2}$ = 20 s at 20°C) is similar to that for channel inactivation seen in our experiments.

The time constant of channel inactivation (~30 s) is too slow to be responsible for the rapid decline of IP_3-stimulated Ca^{2+} release, observed in oocytes (Parker et al., 1996) and other cell types (Meyer and Stryer, 1991), which may be due to inhibition of IP_3R by high local cytoplasmic $[Ca^{2+}]$ generated by the opening of the IP_3R (Parker and Ivorra, 1990). However, the Ca^{2+}-independent inactivation we observed may be involved in suppressing the reopening of the IP_3R as the local $[Ca^{2+}]$ decreases (Hajnóczky and Thomas, 1994), thus allowing the full dissipation of one $[Ca^{2+}]$ spike before the next cycle of $[Ca^{2+}]$ oscillation (Jacob et al., 1988; Wakui et al., 1989; Parker and Yao, 1991). Further experimentation will be required to determine whether the decline in channel activity we observed is due to true inactivation involving an inactivated state I_{irr} of the channel rather than run-down, and to define the mechanisms which enable the receptor to escape from this inactivated state.

Spatial Distribution of IP_3R

Of 740 membrane patches tested, only 102 showed characteristic IP_3R channel activity. It is unlikely that the low P_d was caused by formation of membrane vesicles at the tips of the micropipettes (Hamill et al., 1981) because 150 of our patches exhibited other ion channel activities. Of these, 22 showed IP_3R activities as well, giving a similar P_d (= 0.15) compared with all 740 patches.

We monitored the spatial distribution of functional IP_3R by patch clamping over a wide area of the nuclear envelope and mapping the sites of channel activity. Based on this functional readout, we detected groupings of IP_3R in two different spatial scales. The high frequency of obtaining membrane patches containing multiple IP_3R channels (>8 in some cases), despite the low overall P_d, suggests that the IP_3R tends to aggregate into clusters (Fig. 3). However, in 26 of 59 patches with more than two current levels, attempts to repeatedly patch the same location failed to yield additional patches containing IP_3R channels. Thus, these "micro" IP_3R clusters are probably limited to less than 2 μm in diameter. Transient localized increases of cytoplasmic $[Ca^{2+}]$ imaged in the vicinity of the ER just beneath the plasma membrane of intact *Xenopus* oocytes (Parker and Yao, 1991; Yao et al., 1995) may also be consistent with a patchy distribution of IP_3R in clusters. If these "puffs" were caused by the release of Ca^{2+} from the ER by the opening of IP_3R, the Ca^{2+} current associated with one such Ca^{2+} "puff" is estimated to be ~11 to 23 pA (Yao et al., 1995). With the Ca^{2+} current through unitary IP_3R under physiological conditions estimated to be ~0.5 pA (Bezprozvanny and Ehrlich, 1994), a Ca^{2+} puff would therefore be generated by the cooperative opening of a cluster of IP_3R channels. Because of the considerable uncertainties in estimating variables like endogenous Ca^{2+} buffering capacity of the oocyte cytoplasm and the intralumenal free $[Ca^{2+}]$ in the ER, which were used in computing Ca^{2+} currents associated with a Ca^{2+} puff and a single IP_3R channel, the number of IP_3R channels that form a single Ca^{2+} release site in the oocyte ER may not be significantly different from the maximum number of IP_3R channels (~8) we observed in our multi-channel patches. The recent observations of Ca^{2+} "blips" with amplitudes approximately one-fifth or less of those of "puffs" and their interpretation as representations of unitary IP_3R Ca^{2+} currents (Parker and Yao, 1996) is consistent with our observations of membrane patches with one to over eight IP_3R channels, and therefore suggests a similar organization of IP_3R in the nuclear envelope and ER in oocytes.

Besides the microscopic IP_3R clusters, our experimental results suggest that, at least in some oocyte nuclei, there can also exist a large-scale heterogeneous distribution of functional IP_3R with active areas that may extend over several or even tens of micrometers. In such "macro" clusters, membrane patches containing IP_3R channels, frequently multiple channels, could be repeatedly obtained with P_d close to 1. The grouping of IP_3R into such "hot regions" is reminiscent of the self-organization into large-scale arrays of the ryanodine receptor (Takekura et al., 1995), the Ca^{2+} channel in muscle cells which has partial sequence homology with the IP_3R (Mignery et al., 1989). However, it is possible that the IP_3R in the outer nuclear membrane is actually randomly distributed with a high density, but rarely functional except in the active regions. The IP_3R has been immunolocalized in the nuclear envelope of *Xenopus* oocytes (Parys et al., 1992; Kume et al., 1993; Callamaras and Parker, 1994; Parys et al., 1994; Stehno-Bittel et al., 1995), but the resolution was insufficient to discern uneven IP_3R distribution.

By demonstrating IP_3R channel clustering, our results support the suggestion that heterogeneity of IP_3R channel density among Ca^{2+} stores (Hirose and Iino, 1994) could contribute to the increment detection mechanism observed for Ca^{2+} mobilization by IP_3 (Muallem et al., 1989; Meyer and Stryer, 1990; Taylor and Potter, 1990). Two mechanisms, the Ca^{2+}-independent inactivation of IP_3R in the continuous presence of a supramaximal concentration of IP_3 (present data; Hajnóczky and Thomas, 1994) and the inhibition of Ca^{2+} release by elevated cytoplasmic [Ca^{2+}] (Bezprozvanny et al., 1991; Iino and Endo, 1992; Marshall and Taylor, 1993), might limit the amount of Ca^{2+} that can be released from a Ca^{2+} store before the store is depleted, depending upon the kinetics of inactivation and the magnitude of the Ca^{2+} fluxes. A heterogeneous distribution of IP_3R, as our observations suggest, may provide a mechanism to control the magnitude of the Ca^{2+} fluxes among different Ca^{2+} stores in various parts of the cell. For example, when exposed to a submaximal concentration of IP_3, only those stores containing a sufficiently high density of IP_3R will empty before the channels inactivate. Conversely, stores with a low channel density will only be partially emptied, and therefore able to release more Ca^{2+} when the IP_3R channels are activated again. The delay of IP_3R inactivation in regions with high channel density (Fig. 10) might generate a non-linear relationship between channel density and the amount of Ca^{2+} released, providing an amplification mechanism which could increase the number of "quantal" levels and therefore enable finer tuning of increment detection. Thus, the intrinsic inactivation mechanisms of the IP_3R, together with channel clustering, may provide a mechanism to generate quantal release of Ca^{2+} without requiring a dependence of Ca^{2+} release on luminal [Ca^{2+}] or heterogeneous sensitivity of the IP_3R for IP_3 (Bootman, 1994).

Voltage-dependent Behavior of the IP_3R

Our investigations have revealed a complex pattern of voltage dependencies of the gating activities of the IP_3R channel. First, in either the normal or flicker modes, an increase in V_{app} decreased the average open probability by increasing both the frequency and duration of long channel closures. Second, an increase in V_{app} when the channel was in the flicker mode favored occupancy of F_2 over F_1 by simultaneously increasing the average dwell time of F_2 and decreasing that of F_1. Finally, the channel in either mode could be reactivated from an inactive state I_{Vdep} by an increase in V_{app}. To provide a framework for integrating these complex voltage-dependent gating behaviors, we developed the following simple model for channel gating (Fig. 14).

The model assumes, first, that channel opening in both the normal and flicker modes is controlled by the same mechanism (Fig. 9, gate A). This assumption is supported by the observations that (*a*) the dwell time distribution for the closed state (C) of the IP_3R channel in the normal mode is similar to that of the inter-burst quiescent periods in the flicker mode, with the same voltage dependence; and (*b*) the dwell time distribution for the main state (M) of the normal mode is similar to that for the bursts in the flicker mode. Second, the model assumes that flicker activity is generated by a separate and independent mechanism (Fig. 9, gate B) in series with gate A. The channel is closed when either

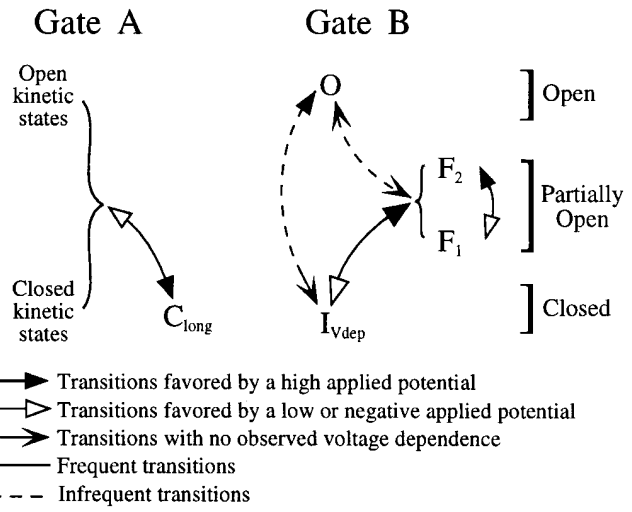

FIGURE 14. Schematic diagram of the double-gate model, showing transitions, especially voltage-dependent ones, between various kinetic states for the two gates controlling the kinetic behavior of the IP_3R channel.

gate is closed, and is open only when both gates are open (completely or partially). In the normal mode, gate B is in a completely open kinetic state (O) and the channel gating is determined entirely by gate A. Gate A has at least two open and at least three closed kinetic states, as revealed by dwell time analysis of the channel in normal mode. The precise transition scheme among these kinetic states has yet to be determined. Only the transition into and out of the long closed kinetic state C_{long} is voltage dependent. A high V_{app} increases the rate of transition into state C_{long} and decreases the rate of transition out of it, thus increasing both the frequency and duration of the long quiescent periods in the normal mode, and the inter-burst periods in the flicker mode.

In this scheme, the channel exhibits flicker behavior when gate B leaves the completely open state O and enters two partially open states, with different conductances corresponding to the F_1 and F_2 states. Transitions between F_1 and F_2 are rapid, involving a relatively low activation energy barrier and, therefore, causing the flickering characteristics, as well as voltage dependent, with a high V_{app} increasing the rate of transition $F_1 \rightarrow F_2$ and decreasing the rate of $F_2 \rightarrow F_1$.

Because most of the channels entered the flicker mode after being reactivated by an increase in V_{app} from the inactive state I_{Vdep} ($n = 13$ out of 17 reactivations), the model includes I_{Vdep} as a kinetic state of gate B, with an increase in V_{app} favoring the transition of I_{Vdep} into F_1 and F_2 (Fig. 14). This model predicts that a decrease in V_{app} will cause the gate to enter the inactive state I_{Vdep}, which agrees with the observations that (*a*) the channel was never detected in the flicker mode under negative V_{app}; and (*b*) when the channel was in the flicker mode, a change of V_{app} from positive to negative closed the channel completely until V_{app} was reversed to positive again.

In this model, gate B is usually in state O since the channel is usually observed in the normal mode. Thus, state O of gate B must be kinetically stable. This stability inhibits gate B from closing readily from O to I_{Vdep} under negative V_{app}, even though I_{Vdep} may be energetically more favorable under negative V_{app}. Thus, unlike in the flicker mode, the channel in the normal mode could be observed under negative V_{app}, with gate B staying in state O.

The model is obviously incomplete. The rarity of conductance states H, S, and L prevents their incorporation into the model, and since the evidence for current level D being a real state of IP_3R is not conclusive, that current level was also left out. It is also unclear how the irreversible inactivated state I_{irr} fits into the model. The fact that the channel activity duration histogram could be fitted with a single exponential component suggests that there is probably one major inactivation pathway to one kinetic state I_{irr}, which could in principle be caused by the irreversible closing of either gate A or gate B, or could involve an independent gating mechanism. Nevertheless, the two-gate model proposed here can account for much of the single-channel gating behavior of the IP_3R we observed, especially those with voltage dependence. Therefore, it provides a framework for developing hypotheses for future experiments.

Along those lines, what might be the nature of gates A and B? IP_3R gating in the normal kinetic mode has been observed in native membranes (Mak and Foskett, 1994; present results; Stehno-Bittel et al., 1995), or in artificial lipid bilayers (Ehrlich and Watras, 1988; Bezprozvanny et al., 1991, 1994; Mayrleitner et al., 1991, 1995; Watras et al., 1991; Bezprozvanny and Ehrlich, 1993, 1994), although the kinetic properties observed differed, possibly because of environmental factors. Thus, we speculate that gate A is intrinsic to the channel, with the various closed and main kinetic states corresponding to different conformations of the IP_3R molecule. In contrast, those states involving gate B, i.e., F_1, F_2, and I_{Vdep}, have been observed only in our experiments, with the IP_3R relatively unperturbed in its native membrane environment. Therefore, it is possible that gate B reflects an accessory molecule associated with the IP_3R molecule which is lost during reconstitution. It is interesting to note that the flicker kinetics of the IP_3R channel are reminiscent of the ion and drug-induced flickering blocks in other channels (Neher and Steinbach, 1978; Fukushima, 1982). Recent results support the notion that accessory molecules might contribute to the kinetic behavior of intracellular Ca^{2+} release channels. Both the ryanodine receptor (Jayaraman et al., 1992; Timerman et al., 1996) and IP_3R (Cameron et al., 1995) are associated stoichiometrically with FKBP12, a ubiquitous 12-kD protein. FKBP12 binding to the ryanodine receptor is associated with marked changes in the gating properties of the channel (Ahern et al., 1994; Chen et al., 1994; Ma et al., 1995) which may reflect, under some conditions, the kinetics of FKBP12 moving into and out of the channel pore under the influence of trans-membrane electric field (Ma et al., 1995). By analogy, FKBP12 or another protein may be an accessory molecule that constitutes gate B in our model, a hypothesis which will require further investigation.

We thank Dr. Peter Drain, Dr. Paul DeWeer and Shawn Wilcox for comments on the manuscript.

Supported by grants from the Medical Research Council of Canada, the NIH and the Cystic Fibrosis Foundation.

Original version received 14 November 1996 and accepted version received 24 February 1997.

REFERENCES

Ahern, G.P., P.R. Junankar, and A.F. Dulhunty. Single channel activity of the ryanodine receptor calcium release channel is modulated by FK-506. *FEBS (Fed. Eur. Biochem. Soc.) Lett.* 352:369–374.

Alexandre, J., J.P. Lassalles, and R.T. Kado. 1990. Opening of Ca^{2+} channels in isolated red beet root vacuole membrane by inositol 1,4,5-trisphosphate. *Nature (Lond.).* 343:567–570.

Berridge, M.J. 1993. Inositol trisphosphate and calcium signaling. *Nature (Lond.).* 361:315–325.

Bezprozvanny, I., S. Bezprozvannaya, and B.E. Ehrlich. 1994. Caffeine-induced inhibition of inositol(1,4,5)-trisphosphate-gated calcium channels from cerebellum. *Mol. Biol. Cell.* 5:97–103.

Bezprozvanny, I., and B.E. Ehrlich. 1993. ATP modulates the function of inositol 1,4,5-trisphosphate-gated channels at two sites. *Neuron.* 10:1175–1184.

Bezprozvanny, I., and B.E. Ehrlich. 1994. Inositol (1,4,5)-trisphosphate ($InsP_3$)-gated Ca channels from cerebellum: conduction properties for divalent cations and regulation by intraluminal calcium. *J. Gen. Physiol.* 104:821–856.

Bezprozvanny, I., J. Watras, and B.E. Ehrlich. 1991. Bell-shaped calcium-response curves of $Ins(1,4,5)P_3$- and calcium-gated channels from endoplasmic reticulum of cerebellum. *Nature (Lond.).* 351:751–754.

Bootman, M.D. 1994. Quantal Ca^{2+} release from $InsP_3$-sensitive intracellular stores. *Mol. Cell. Endocrinol.* 98:157–166.

Bustamante, J.O. 1992. Nuclear ion channels in cardiac myocytes. *Pflügers Arch.* 421:473–485.

Bustamante, J.O. 1993. Restricted ion flow at the nuclear envelope of cardiac myocytes. *Biophys. J.* 64:1735–1749.

Bustamante, J.O. 1994. Open states of nuclear envelope ion channels in cardiac myocytes. *J. Membr. Biol.* 138:77–89.

Callamaras, N., and I. Parker. 1994. Inositol 1,4,5-trisphosphate receptors in *Xenopus laevis* oocytes: localization and modulation by Ca^{2+}. *Cell Calcium.* 15:66–78.

Cameron, A.M., J.P. Steiner, D.M. Sabatini, A.J. Kaplan, L.D. Walensky, and S.H. Snyder. 1995. Immunophilin FK506 binding protein associated with inositol 1,4,5-trisphosphate receptor modulates calcium flux. *Proc. Natl. Acad. Sci. USA.* 92:1784–1788.

Chen, S.R.W., L. Zhang, and D.H. MacLennan. 1994. Assymmetrical blockage of the Ca^{2+} release channel (ryanodine receptor) by 12-kDa FK506 binding protein. *Proc. Natl. Acad. Sci. USA.* 91: 11953–11957.

Colquhoun, D., and F.J. Sigworth. 1995. Fitting and statistical analysis of single-channel records. *In* Single-Channel Recording. 2nd edition. B. Sakmann and E. Neher, editors. Plenum Press, New York. 483–588.

Coquil, J.-F., J.-P. Mauger, and M. Claret. 1996. Inositol 1,4,5-trisphosphate slowly converts its receptor to a state of higher affinity in sheep cerebellum membranes. *J. Biol. Chem.* 271:3568–3574.

Coronado, R., and R. Latorre. 1983. Phospholipid bilayers made from monolayers on patch-clamp pipettes. *Biophys. J.* 43:231–236.

Dingwall, C., and R. Laskey. 1992. The nuclear membrane. *Science (Wash. DC).* 258:942–947.

Ehrlich, B.E., and J. Watras. 1988. Inositol 1,4,5-trisphosphate activates a channel from smooth muscle sarcoplasmic reticulum. *Nature (Lond.).* 336:583–586.

Finch, E.A., T.J. Turner, and S.M. Goldin. 1991. Calcium as a coagonist of inositol 1,4,5-trisphosphate-induced calcium release. *Science (Wash. DC).* 252:443–446.

Fukushima, Y. 1982. Blocking kinetics of the anomalous potassium rectifier of tunicate egg studied by single channel recording. *J. Physiol. (Lond.).* 331:311–331.

Hajnóczky, G., and A.P. Thomas. 1994. The inositol trisphosphate calcium channel is inactivated by inositol trisphosphate. *Nature (Lond.).* 370:474–477.

Hamill, O.P., A. Marty, E. Neher, B. Sakmann, and F. Sigworth. 1981. Improved patch-clamp techniques for high-resolution current recording from cells and cell-free membrane parches. *Pflügers Arch.* 391:85–100.

Hilly, M., F. Piétri-Rouxel, J.-F. Coquil, M. Guy, and J.-P. Mauger. 1993. Thiol reagents increase the affinity of the inositol 1,4,5-trisphosphate receptor. *J. Biol. Chem.* 268:16488–16494.

Hirose, K., and M. Iino. 1994. Heterogeneity of channel density in inositol 1,4,5-trisphosphate-sensitive Ca^{2+} stores. *Nature (Lond.).* 372:791–794.

Iino, M., and M. Endo. 1992. Calcium-dependent immediate feedback control of inositol 1,4,5-trisphosphate-induced Ca^{2+} release. *Nature (Lond.).* 360:76–78.

Jacob, R., J.E. Merritt, T.J. Hallam, and T.J. Rink. 1988. Repetitive spikes in cytoplasmic calcium evoked by histamine in human endothelial cells. *Nature (Lond.).* 335:40–45.

Jayaraman, T., A.-M. Brillantes, A.P. Timerman, S. Fleischer, H. Erdjument-Bromage, P. Tempst, and A.R. Marks. 1992. FK506 binding protein associated with the calcium release channel (ryanodine receptor). *J. Biol. Chem.* 267:9474–9477.

Joseph, S.K. 1996. The inositol trisphosphate receptor family. *Cell Signaling.* 8:1–7

Kaplin, A.I., C.D. Ferris, S.M. Voglmaier, and S.H. Snyder. 1994. Purified reconstituted inositol 1,4,5-trisphosphate receptors. Thiol reagents act directly on receptor protein. *J. Biol. Chem.* 269: 28972–28978.

Kobrinsky, E., K. Ondrias, and A.R. Marks. 1995. Expressed ryanodine receptor can substitute for the inositol 1,4,5-trisphosphate receptor in *Xenopus laevis* oocytes during progesterone-induced maturation. *Dev. Biol.* 172:531–540.

Kume, S., A. Muto, J. Aruga, T. Nakagawa, T. Michikawa, T. Furuichi, S. Nakade, H. Okano, K. Mikoshiba. 1993. The *Xenopus* IP_3 receptor: structure, function and localization in oocytes and *eggs. Cell.* 73:555–570.

Lin, C., G. Hajnóczky, and A.P. Thomas. 1994. Propagation of cytosolic calcium waves into the nuclei of hepatocytes. *Cell Calcium.* 16:247–258.

Ma, J., M.B. Bhat, and J. Zhao. 1995. Rectification of skeletal muscle ryanodine receptor mediated by FK506 binding protein. *Biophys. J.* 69:2398–2404.

Mak, D.D., and J.K. Foskett. 1994. Single-channel inositol 1,4,5-trisphosphate receptor currents revealed by patch clamp of isolated *Xenopus* oocyte nuclei. *J. Biol. Chem.* 269:29375–29378.

Matzke, A.J.M., C. Behensky, T. Weiger, and M.A. Matzke. 1992. A large conductance ion channel in the nuclear envelope of a higher plant cell. *FEBS (Fed. Eur. Biochem. Soc.) Lett.* 302:81–85.

Mayrleitner, M., C.C. Chadwick, A.P. Timerman, S. Fleischer, and H. Schindler. 1991. Purified IP_3 receptor from smooth muscle forms and IP_3 gated and heparin sensitive Ca^{2+} channel in planar bilayers. *Cell Calcium.* 12:505–514.

Mayrleitner, M., R. Schäfer, and S. Fleischer. 1995. IP_3 receptor purified from liver plasma membrane is an (1,4,5) IP_3 activated and (1,3,4,5) IP_4 inhibited calcium permeable ion channel. *Cell Calcium.* 17:141–153.

Mazzanti, M., L.J. DeFelice, J. Cohen, and H. Malter. 1990. Ion channels in the nuclear envelope. *Nature (Lond.).* 343:764–767.

Mazzanti, M., L.J. DeFelice, and E.F. Smith. 1991. Ion channels in murine nuclei during early development and in fully differentiated adult cells. *J. Membr. Biol.* 121:189–198.

Meyer, T., and L. Stryer. 1990. Transient calcium release induced by successive increments of inositol-1,4,5-trisphosphate. *Proc. Natl. Acad. Sci. USA.* 87:3841–3845.

Meyer, T., and L. Stryer. 1991. Calcium spiking. *Annu. Rev. Biophys. Biophys. Chem.* 20:153–174.

Meyer, T., T. Wensel, and L. Stryer. 1990. Kinetics of calcium channel opening by inositol-1,4,5-trisphosphate receptor. *Biochemistry.* 29:32–37.

Mignery, G.A., C.L. Newton, B.T. Archer III, and T.C. Südhof. 1990. Structure and expression of the rat inositol 1,4,5-trisphosphate receptor. *J. Biol. Chem.* 265:12679–12685.

Mignery, G.A., and T.C. Südhof. 1990. The ligand binding site and transduction mechanism in the inositol-1,4,5-trisphosphate receptor. *EMBO (Eur. Mol. Biol. Organ.) J.* 9:3893–3898.

Mignery, G.A., T.C. Südhof, K. Takei, and P. De Camilli. 1989. Putative receptor for inositol-1,4,5-trisphosphate similar to ryanodine receptor. *Nature (Lond.).* 342:192–195.

Mikoshiba, K. 1993. Inositol 1,4,5-trisphosphate receptor. *Trends Pharmacol. Sci.* 14:86–89.

Missiaen, L., J.B. Parys, H. de Smedt, B. Himpens, and R. Casteels. 1994. Inhibition of inositol trisphosphate-induced calcium release by caffeine is prevented by ATP. *Biochem. J.* 300:81–84.

Miyazaki, S. 1988. Inositol 1,4,5-trisphosphate-induced calcium release and guanine nucleotide-binding protein-mediated periodic calcium rises in golden hamster eggs. *J. Cell Biol.* 106:345–353.

Muallem, S., S.J. Pandol, and T.G. Beeker. 1989. Hormone-evoked calcium release from intracellular stores is a quantal process. *J. Biol. Chem.* 264:205–212.

Neher, E., and J.H. Steinbach. 1978. Local anaesthetics transiently block currents through single acetylcholine-receptor channels. *J. Physiol. (Lond.).* 277:153–176.

Parker, I., and I. Ivorra. 1990. Inhibition by Ca^{2+} of inositol trisphosphate-mediated liberation: A possible mechanism for oscillatory release of Ca^{2+}. *Proc. Natl. Acad. Sci. USA.* 87:260–264.

Parker, I., and Y. Yao. 1991. Regenerative release of calcium from functionally discrete subcellular stores by inositol trisphosphate. *Proc. Royal Soc. B.* 246:269–274.

Parker, I., Y. Yao, and V. Ilyin. 1996. Fast kinetics of calcium liberation induced in *Xenopus* oocytes by photoreleased inositol trisphosphate. *Biophys. J.* 70:222–237.

Parys, J.B., S.M. McPherson, L. Mathews, K.P. Campbell, and F.J. Longo. 1994. Presence of inositol 1,4,5-trisphosphate receptor, calreticulin, and calsequestrin in eggs of sea urchins and *Xenopus laevis*. *Dev. Biol.* 161:466–476.

Parys, J.B., S.W. Sernett, S. DeLisle, P.M. Snyder, M.J. Welsh, and K.P. Campbell. 1992. Isolation, characterization, and localization of the inositol 1,4,5-trisphosphate receptor protein in *Xenopus laevis oocytes. J. Biol. Chem.* 267:18776–18782.

Pasyk, E.A., and J.K. Foskett. 1995. Mutant (ΔF508) cystic fibrosis transmembrane conductance regulator Cl^- channel is functional when retained in endoplasmic reticulum of mammalian cells. *J. Biol. Chem.* 270:12347–12350.

Percival, A.L., A.J. Williams, J.L. Kenyon, M.M. Brinsell, J.A. Airey, and J.L. Sutko. 1994. Chicken skeletal muscle ryanidine receptor isoforms: ion channel properties. *Biophys. J.* 67:1834–1850.

Piétri, F., M. Hilly, and J.-P. Mauger. 1990. Calcium mediates the interconversion between two states of the liver inositol 1,4,5-trisphosphate receptor. *J. Biol. Chem.* 265:17478–17485.

Putney, J.W., Jr., and G.St.J. Bird. 1993. The Inositol phosphate-calcium signaling system in nonexcitable cells. *Endocr. Rev.* 14:610–631.

Root, M.J., and R. MacKinnon. 1994. Two identical noninteracting sites in an ion channel revealed by proton transfer. *Science (Wash. DC).* 265:1852–1856.

Sakmann, B., and E. Neher. 1995. Geometric parameters of pipettes and membrane patches. *In* Single-Channel Recording. 2nd edition. B. Sakmann and E. Neher, editors. Plenum Press, New York. 637–650.

Sigworth, F.J., and S.M. Sine. 1987. Data transformations for improved display and fitting of single-channel dwell time histograms. *Biophys. J.* 52:1047–1054.

Smith, J., R. Coronado, and G. Meissner. 1986. Single-channel measurements of the calcium release channel from skeletal muscle sarcoplasmic reticulum. Activation by Ca^{2+} and ATP and modulation by Mg^{2+}. *J. Gen. Physiol.* 88:573–588.

Smith, L.D., W. Xu, and R.L. Varnold. 1991. Oogenesis and oocyte isolation. *In* Methods in Cell Biology. Vol. 36 *Xenopus laevis:* Practical Uses in Cell and Molecular Biology. B.N. Kay and H.B. Peng, editors. Academic Press, San Diego. 45–61.

Somlyo, A.V., H. Shuman, and A.P. Somlyo. 1977. Elemental distribution in striated muscle and effects of hypertonicity: electron probe analysis of cryosections. *J. Cell Biol.* 74:828–857.

Stehno-Bittel L., A. Lückhoff, and D.E. Clapham. 1995. Calcium release from the nucleus by $InsP_3$ receptor channels. *Neuron.* 14: 163–167.

Supattapone, S., P.F. Worley, J.M. Baraban, and S.H. Snyder. 1988. Solubilization, purification and characterization of an inositol trisphosphate receptor. *J. Biol. Chem.* 263:1530–1534.

Tabares, L., M. Mazzanti, and D.E. Clapham. 1991. Chloride channels in the nuclear membrane. *J. Membr. Biol.* 123:49–54.

Takekura, H., H. Takeshima, S. Nishimura, M. Takahashi, T. Tanabe, V. Flockerzi, F. Hofmann, and C. Franzini-Armstrong. 1995. Co-expression in CHO cells of two muscle proteins involved in excitation-contraction coupling. *J. Muscle Res. Cell Motility.* 16:465–480.

Taylor C.W., and B.V.L. Potter. 1990. The size of inositol 1,4,5-trisphosphate-sensitive Ca^{2+} store depends on inositol 1,4,5-trisphosphate concentration. *Biochem. J.* 266:189–194.

Taylor C.W., and A. Richardson. 1991. Structure and function of inositol trisphosphate receptors. *Pharmac. Ther.* 51:97–137.

Taylor, C.W., and D. Traynor. 1995. Calcium and inositol trisphosphate receptors. *J. Membr. Biol.* 145:109–118.

Timerman, A.P., H. Onoue, H.-B. Xin, S. Barg, J. Copello, G. Wiederrecht, and S. Fleischer. 1996. Selective binging of FKPB12.6 by the cardiac ryanodine receptor. *J. Biol. Chem.* 271:20385–20391.

Thrower, E., H. Duclohier, E.J.A. Lea, G. Molle, and A.P. Dawson. 1996. The inositol 1,4,5-trisphosphate-gated Ca^{2+} channel: effect of the protein thiol reagent thimerosal on channel activity. *Biochem. J.* 318:61–66.

Wakui, M., B.V.L. Potter, and O.H. Petersen. 1989. Pulsatile intracellular calcium release does not depend on fluctuations in inositol trisphosphate concentration. *Nature (Lond.).* 339:317–320.

Watras J., I. Bezprozvanny, and B.E. Ehrlich. 1991. Inositol 1,4,5-trisphosphate-gated channels in cerebellum: presence of multiple conductance states. *J. Neuroscience.* 11:3239–3245.

Watras, J., I. Moraru, D.J. Costa, and L.A. Kindman. 1994. Two inositol 1,4,5-trisphosphate binding sites in rat basophilic leukemia cells: relationship between receptor occupancy and calcium release. *Biochemistry.* 33:14359–14367.

Williams, A.J. 1992. Ion conduction, and discrimination in the sarcoplasmic reticulum ryanodine receptor/calcium-release channel. *J. Muscle Res. Cell Motility.* 13:7–26.

Yamamoto-Hino, M., T. Sugiyama, K. Hikichi, M.G. Mattei, K. Hasegawa, S. Sekine, K. Sakurada, A. Miyawaki, T. Furuichi, M. Hasegawa, and K. Mikoshiba. 1994. Cloning and characterization of human type 2 and type 3 inositol 1,4,5-trisphosphate receptors. *Receptors and Channels.* 2:9–22.

Yao Y., J. Choi, and I. Parker. 1995. Quantal puffs of intracellular Ca^{2+} evoked by inositol trisphosphate in *Xenopus oocytes. J. Physiol.* 482:533–553.